**Steel and Composite Structures**, *Vol. 35, No. 5 (2020) 611-625*
DOI: https://doi.org/10.12989/scs.2020.35.5.611


# Experimental and numerical studies on the behaviour of corroded cold-formed steel columns

Nie Biao*, Xu Shanhua, Zhang Haijiang and Zhang Zongxing

*School of Civil Engineering, Xi'an University of Architecture & Technology, No.13, middle section of Yanta Road, Beilin District, China*

(*Received January 15, 2020, Revised April 28, 2020, Accepted May 13, 2020*)

**Abstract.** Experimental investigation and finite element analysis of corroded cold-formed steel (CFS) columns are presented. 11 tensile coupon specimens and 6 stub columns of corroded CFS that had a channel section of C160x60x20 were subjected to monotonic tensile tests and axial compression tests, respectively. The degradation laws of the mechanical properties of the tensile coupon specimens and stub columns were analysed. An appropriate finite element model for the corroded CFS columns was proposed and the influence of local corrosion on the stability performance of the columns was studied by finite element analysis. Finally, the axial capacity of the experimental results was compared with the predictions obtained from the existing design specifications. The results indicated that with an increasing average thickness loss ratio, the ultimate strength, elastic modulus and yield strength decreased for the tensile coupon specimens. Local buckling deformation was not noticeable until the load reached about 90% of the ultimate load for the non-corroded columns, while local buckling deformation was observed when the load was only 40% of the ultimate load for the corroded columns. The maximum reduction of the ultimate load and critical buckling load was 57% and 81.7%, respectively, compared to those values for the non-corroded columns. The ultimate load of the columns with web thickness reduced by 2 mm was 53% lower than that of the non-corroded columns, which indicates that web corrosion most significantly affects the bearing capacity of the columns with localized corrosion. The results predicted using the design specifications of MOHURD were more accurate than those predicted using the design specifications of AISI.

**Keywords:** cold-formed steel; mechanical properties; corrosion; finite element analysis; columns

## 1. Introduction

For steel structures exposed to corrosive environments, including hot and humid environments, acidic or chloride-rich environments and industrial environments, the corrosion damage, which results in a significant reduction in the mechanical properties of steel (Xu *et al*. 2019a, Wang *et al*. 2017, Wang *et al*. 2020a, Garbatov *et al*. 2014) has become a predominant factor affecting the safety and durability of steel structures, even if they are protected by protective measures. According to relevant statistical data, China's annual economic loss due to steel corrosion is 70 billion US dollars, of which 14 billion US dollars is lost in the construction industry. Steel corrosion not only causes economic loss and waste of resources, but also has a significant impact on the service and safety performance of steel structures.

In recent years, several experiments have been conducted to study the effect of corrosion damage on the mechanical properties of the corroded steel plates. To obtain corroded steel plates with an acceptable processing time, some methods have been proposed to replace natural corrosion, such as the accelerated corrosion method (Qiu and Xu, 2014; Qin *et al*. 2016; Li *et al*. 1999) and artificial mechanical method (Sheng *et al*. 2017). Research has shown that the accelerated corrosion method and artificial mechanical method can simulate the effect of long-term natural corrosion (Melchers and Wells 2006, Nakai 2004) . Garbatov *et al.* (2014) used the volume loss rate to characterize the degree of degradation and established regression equations derived for the elasticity modulus, tensile strength, yield stress and total uniform elongation as a function of the volume loss rate. The corrosion degree was determined based on the mass loss ratio by Qiu *et al.* (2014) and the results show that when the mass loss ratio was not more than 4%, the corrosion has no significant effect on the yield strength and tensile strength. When the mass loss ratio was more than 4%, the yield strength and tensile strength decreased linearly with increasing mass loss ratio. The elongation showed an obvious degradation trend with the increase of mass loss ratio. The degree of pit corrosion intensity (DOP) was adopted to evaluate the scale of damage by Paik *et al.* (2003), through which the relationship between the ultimate strength of the steel plates and the DOP was proposed. The surface topography of the corroded steel plates was measured by Qin *et al.* (2016) and the variation of the surface characteristic parameters (void ratio, average corrosion depth, maximum corrosion depth, surface roughness) as a function of the mass loss ratio was established.

Beaulieu *et al.* (2010) carried out an axial compression test on 16 steels angle corroded by the accelerated corrosion method (the galvanic corrosion process) and believed that

*Corresponding author, Ph.D.
E-mail: xnniebiao@163.com



ISSN: 1229-9367 (Print), 1598-6233 (Online)

the existing design specifications did not accurately predict the compressive capacity of the corroded steel angle members after comparing the experimental data and results predicted by the existing design equations based on the average residual thickness. Karagah *et al.* (2015) studied the effect of localized corrosion simulated by milling the flanges or web on the axial compressive capacity of H-shaped stub columns that were used in bridge construction. The results show that the decrease in the load-carrying capacity of stub columns with localized corrosion was linearly related to the decrease in the minimum cross-section area. The remaining axial capacity can be calculated by multiplying the capacity predicted by the existing design specifications for a non-corroded column by section loss ratio. Shi *et al.* (2014) used the non-linear finite element method to study the inelastic buckling of H-shaped stub columns with localized corrosion and compared the numerical results and results predicted using three different design specifications. The effective width method was more suitable for calculating the load-carrying capacity of the severely corroded columns and the AASHTO and DSM provided the most accurate prediction for the mildly corroded columns. Cinitha *et al.* (2014) carried out an experimental study on corroded steel compression members (angle and tubular specimens) obtained by the galvanostatic method. The compression test on the corroded members shows that the corrosion location and thickness, weight loss have a significant effect on the mechanical properties. The mechanical properties of other corroded steel members have also been extensively studied, such as steel tubular members (Cinitha *et al.* 2018, Wang *et al.* 2018), steel plate girders (Kim *et al.* 2013, Khurram *et al.* 2014), steel beams (Sharifi and Rahgozar 2010, Rahgozar 2009), steel beams (Wang *et al*., (2020b)) and steel box girders (Saad-Eldee *et al.* 2012).

Light gauge CFS structure has been widely used in construction engineering due to its energy savings, environmental friendliness and great economic benefits (Zhou and Chen 2018, Roy *et al.* 2019a, Ananthi *et al.* 2019). Many researchers have done a lot of research on CFS without corrosion (Chen *et al.* 2019, Roy *et al.* 2018, Roy *et al.* 2019b, Ananthi *et al.* 2019). CFS increases the bearing capacity of members by changing the section form rather than increasing the thickness, which can save material while ensuring structural safety. To prevent corrosion of CFS, hot-dip galvanizing is often used. However, many CFS structure are seriously corroded in practical engineering (Zhang *et al*. 2019, Xu *et al*. 2019a). Research shows that the cold-working process can accelerate the corrosion of steel structures (Štefec *et al.* 1978, Nakhaie and Moayed 2014). Štefec *et al.* (1978) analysed the distribution and size of pitting corrosion of steel with different degrees of cold-working through the corrosion test and the results showed that cold-working greatly increased the pitting area. At present, much research has been conducted on corroded hot-rolled steel, but there is little research on corroded CFS, especially corroded CFS columns. To study the effect of corrosion on the mechanical properties of a CFS plate, a monotonic tensile test on flat and corner coupon specimens from iron and steel works was performed, and a constitutive model for corroded CFS considering the sectional loss ratio was proposed (Nie *et al.* 2019).

The objective of this study was to investigate the compression performance of the corroded CFS columns that had a channel section of C160x60x20. The thickness distribution, failure mode, load-strain curve, load-displacement curve, axial displacement corresponding to the ultimate load, critical buckling load and ultimate load were obtained by taking thickness measurements and performing axial compression tests. A finite element model for the corroded CFS columns was established and a series of parametric analyses were performed on the local corrosion of the CFS columns. Finally, the remaining axial capacity obtained by the experimental results was compared with the results calculated by the existing design specifications.

## 2. Mechanical properties of corroded CFS

All specimens, including tensile coupon specimens and stub columns, came from CFS channel sections of C160x60x20 that had been in service for 4 years in an electrolysis factory (shown in Fig. 1). It can be seen from Fig. 1 that the CFS had been seriously corroded, although they had not been used for a long period of time. The CFS (low-alloy steel (Q345)) was made by using a press brake machine on galvanized steel sheets with a nominal plate thickness of 2.5 mm.

Tensile coupon specimens, whose dimensions are presented in Fig. 2, were cut from the web of the corroded CFS. Eleven specimens with different degrees of corrosion were manufactured and subjected to a monotonic tensile test to obtain the stress-strain relationships and mechanical properties. The average thickness loss ratio used as a damage parameter for corrosion could be expressed as follows

$$\eta = \frac{h_a}{h_0} \tag{1}$$

Fig. 1 Experimental materials

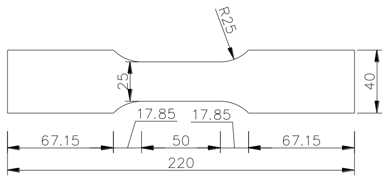


Fig. 2 Dimensions of the tensile coupon specimens(mm)

where $h_a$ is the average thickness of the corroded specimens, $h_0$ is the original thickness, $\eta$ is the average thickness loss ratio.

The average thickness loss ratio and mechanical properties (elastic modulus, yield strength and ultimate strength) were obtained based on the average cross-sectional area, as shown in Table 1. The test results showed that as average thickness loss ratio increased, the elastic modulus, yield strength and ultimate strength decreased. The corrosion reduction factor was calculated as the ratio of the mechanical properties (elastic modulus and yield strength) of the corroded specimens to that of the non-corroded specimens. Fig. 3 shows that the relationship between the corrosion reduction factor for elastic modulus (a) and yield strength (b) and the average thickness loss ratio. The specimen (F4) with a 38.9% reduction in the average thickness loss showed a 43.53% decrease in the elastic modulus and a 49.31% reduction in the yield strength compared to the non-corroded specimens. In addition, the corrosion reduction factor of the elastic modulus and yield strength could be expressed as follows

$$\frac{E_s}{E_{s0}} = 1 - 6 * 10\text{^}{-4} * \exp\left(\eta / 0.693\right) \tag{2}$$

$$\frac{f_y}{f_{y0}} = 1 - 0.648 * \eta \tag{3}$$

where $E_s$ is the elastic modulus of the corroded specimens, $E_{s0}$ is the elastic modulus of the non-corroded specimens, $f_y$ is the yield strength of the corroded specimens, $f_{y0}$ is the yield strength of the non-corroded specimens

Table 1 Mechanical properties of the tensile coupon specimens

| Specimen | $\eta$ | $E_s(10^3)$(N/mm$^2$) | $f_y$(MPa) | $f_u$(MPa) |
|---|---|---|---|---|
| F1 | 0 | 198.99 | 354.90 | 444.32 |
| F2 | 0.127 | 196.45 | 331.96 | 422.56 |
| F3 | 0.580 | 162.53 | 209.06 | 333.18 |
| F4 | 0.611 | 112.35 | 179.94 | 198.31 |
| F5 | 0.276 | 194.71 | 252.25 | 352.68 |
| F6 | 0.582 | 156.56 | 269.31 | 291.45 |
| F7 | 0.571 | 155.26 | 181.34 | 188.79 |
| F8 | 0.560 | 140.23 | 239.89 | 250.67 |
| F9 | 0.593 | 132.56 | 254.75 | 285.64 |
| F10 | 0.467 | 189.63 | 249.08 | 313.89 |
| F11 | 0.343 | 194.25 | 286.95 | 404.39 |

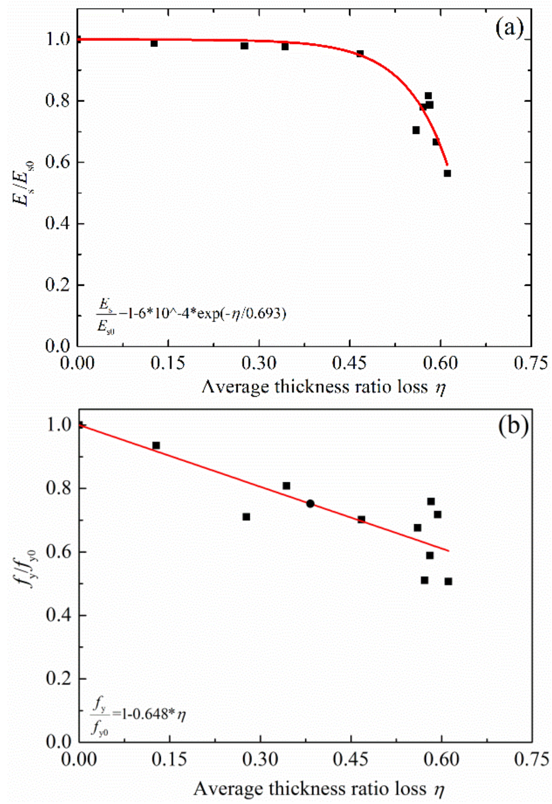


Fig. 3 Elastic modulus (a) and yield strength (b) versus average thickness loss ratio

## 3 Experimental program

### *3.1 Dimensions of the test columns*

According to the results of the monotonic tensile test and dimensions of the columns, a total of 6 CFS stub columns with different corrosion ratios were fabricated with a nominal length of 500 mm (between 3*h* and 20*r*, where *h* is web depth and *r* is least radius of gyration), including 1 non-corroded column (C160-A-1) and five corroded columns (C160-A-2, C160-A-3, C160-A-4, C160-A-5, C160-A-6). An end plate with a nominal thickness of 10 mm was welded to the end of all the columns to obtain uniform compression. The cross-sections of the test columns are presented in Fig. 4. The cross-sectional dimensions of four different positions were measured by a Vernier calliper, and the average values were taken as the cross-sectional dimensions as shown in Table 2.

Corrosion, which is a stochastic process, leads to a different thickness loss at different positions of the columns. For thin-walled structures, a small difference in thickness has a great influence on mechanical properties. Therefore, the thickness at different positions was measured using an ultrasonic thickness gauge (shown in Fig. 5(a)). A cross-section was selected every 50 mm along the length direction (h) for thickness measurements (shown in Fig. 5 (b)), and 9 points on each cross-section were measured, including 5 points on the web (w), 2 points on the flange (f) and 1 point on the lip (l). A total of 99 data points were recorded. Fig. 6

Table 2 Dimensions of the test columns

| Specimen | $l$ (mm) | $h_{1\text{-}1}$ (mm) | $h_{2\text{-}1}$ (mm) | $h_3$ (mm) | $h_{2\text{-}2}$ (mm) | $h_{1\text{-}2}$ (mm) | $s$ (mm) | $b_1$ (mm) | $b_2$ (mm) | $a_1$ (mm) | $a_2$ (mm) | $r$ (mm) |
|---|---|---|---|---|---|---|---|---|---|---|---|---|
| C160-A-1 | 498.2 | 64.3 | 7.8 | 16.1 | 8.1 | 63.2 | 1 | 57.5 | 60.7 | 18.6 | 22.0 | 2.5 |
| C160-A-2 | 500.2 | 63.9 | 8.1 | 15.8 | 7.8 | 62.9 | 1 | 57.25 | 60.7 | 17.0 | 20.6 | 2.5 |
| C160-A-3 | 498.5 | 62.2 | 7.9 | 16.2 | 8.2 | 63.2 | 1 | 57.5 | 60.5 | 18.7 | 19.8 | 2.5 |
| C160-A-4 | 498.5 | 64.4 | 7.9 | 16.1 | 8.1 | 62.7 | 1 | 56.5 | 60.7 | 20.0 | 18.8 | 2.5 |
| C160-A-5 | 499.0 | 64.3 | 8.2 | 15.9 | 7.9 | 63.2 | 1 | 56.2 | 61 | 20.6 | 17.9 | 2.5 |
| C160-A-6 | 498.2 | 61.9 | 7.8 | 16.3 | 8.1 | 63.35 | 1 | 59.7 | 56.7 | 20.5 | 18.3 | 2.5 |

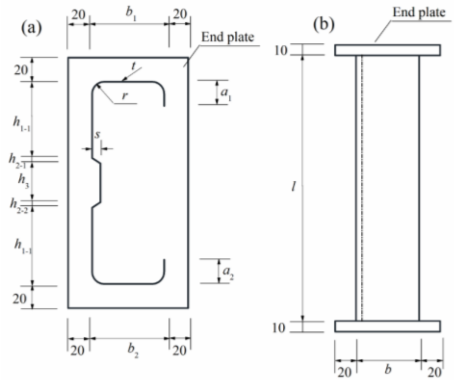


Fig. 4 Cross-sections of the test columns


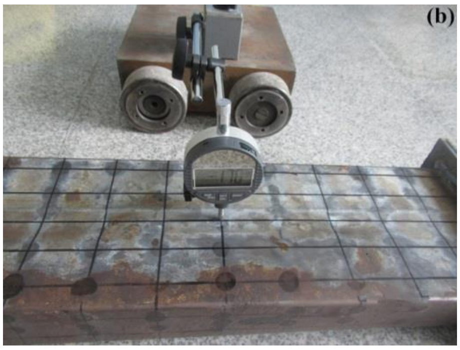


Fig. 5 Thickness (a) and geometric imperfections (b) measuring equipment

shows the thickness distributions of the test columns with different corrosion damage. It can be found from Fig. 6 that the difference in thickness between the different positions was very large and the maximum difference was 1.5 mm, which indicates that the corrosion is highly inhomogeneous. In addition, the loss of web thickness was obviously greater than the loss of flange and lip thickness for the same cross-section.

### *3.2 Initial geometric imperfections*

Initial geometric imperfection is a very important factor for the stability behaviour of light gauge CFS. The local and distortional initial geometric imperfections of all the stub columns were measured by using a dial indicator (shown in Fig. 5(b)). The initial geometric imperfections were measured every 50 mm along the column lengths and 9 points were recorded in each geometric imperfection. The initial geometric imperfections along the column lengths are presented in Fig. 7. $\Delta_w$ and $\Delta_f$ are the local geometric imperfection measurement positions on the web and flanges, respectively and $\Delta_d$ is the distortional geometric imperfection. Negative values represent concave imperfection, while positive values represent convex imperfections. As shown in Fig. 7, the initial geometric imperfections along column length have no obvious regularity, and the maximum local and distortional initial geometric imperfections were 1.48 and 2.14, respectively. This shows that the initial geometric imperfections of the columns in practical engineering were quite large. The maximum initial geometric imperfections are given in Table

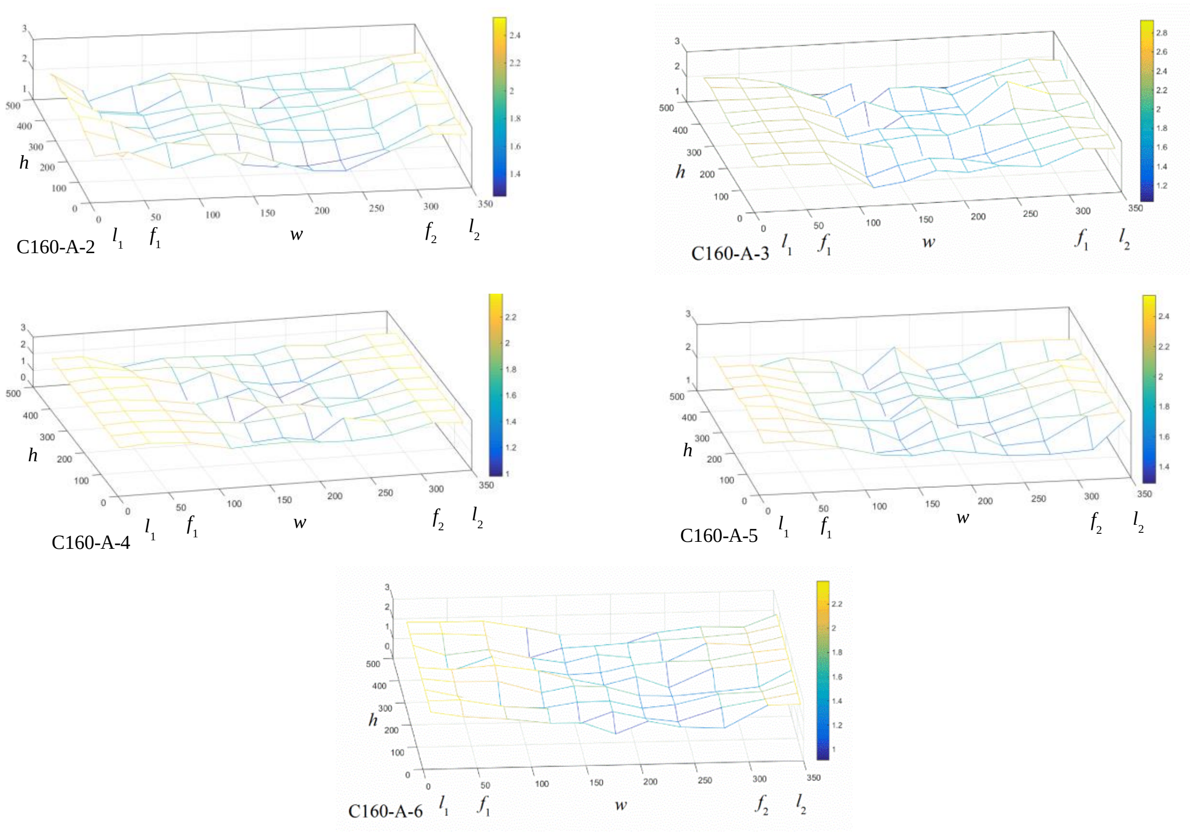


Fig. 6 Thickness distribution of the columns

Table 3 Maximum initial geometric imperfections

| Specimen | $\Delta_{wmax}$ (mm) | $\Delta_{f1max}$ (mm) | $\Delta_{f2max}$ (mm) | $\Delta_{d1max}$ (mm) | $\Delta_{d2max}$ (mm) |
|---|---|---|---|---|---|
| C160-A-1 | 0.55 | -0.14 | -0.50 | 1.34 | -1.38 |
| C160-A-2 | 1.36 | -0.34 | -0.59 | -2.14 | -1.74 |
| C160-A-3 | 1.48 | -0.19 | -0.49 | 2.13 | 1.47 |
| C160-A-4 | 1.36 | -0.23 | -0.58 | 1.72 | 1.84 |
| C160-A-5 | 1.25 | -0.47 | -0.55 | 1.58 | -1.75 |
| C160-A-6 | 0.91 | -0.43 | 0.75 | 1.36 | -1.39 |

3. As shown in Table 3, the initial geometric imperfections of the corroded columns were obviously larger than those of the non-corroded columns, and the distortional geometric imperfection was greater than the local geometric imperfection. The maximum initial geometric imperfections will be applied in a finite element analysis.

### 3.3 Measuring point arrangement

A total of 46 strain gauges were employed to track the buckling behaviour of the columns. 11 pairs (inside and outside) of strain gauges were mounted onto the cross-section at the mid-height of the columns, as shown in Fig. 8 (a). It is difficult to determine the buckling position due to the uneven corrosion along the column length. Therefore, to capture the buckling behaviour, 12 pairs of strain gauges were placed along the length direction of the flange and web centerline at a spacing of 100 mm (shown in Fig. 8 (a)). Two displacement transducers (No. 1 and 2) were placed on the lip at mid-height of the columns to measure the distortional buckling deformation. Displacement transducers No. 2, 4 and 6 were designed to measure the local buckling deformation. Displacement transducers No. 5 and 7 were positioned at the edge of the web to measure the probable overall buckling deformation. Four displacement transducers (No. 8-11) were placed along the length direction of the web centreline at a spacing of 100 mm to measure the possible local buckling deformation (shown in Fig. 8(b)). Finally, the axial shortening was measured by two displacement transducers (No. 12 and 13) placed at the centroid of the two end cross-sections.

### 3.4 Experimental set-up

An axial compression test of the stub columns was conducted using a 5000 kN capacity electro-hydraulic servo pressure testing machine (YAW-5000), as shown in Fig. 9. The top knife edge and bottom knife edge were employed to maintain the pinned-end supports, as shown in Figs. 9(b) and 9(c). After the centroid axes of the stub columns were aligned with that of the knife edge, a pre-compression load was applied. The axial compression test was carried out in displacement control at a rate of 0.05 mm/min. The test was stopped when the load drops to 75% of the ultimate load,

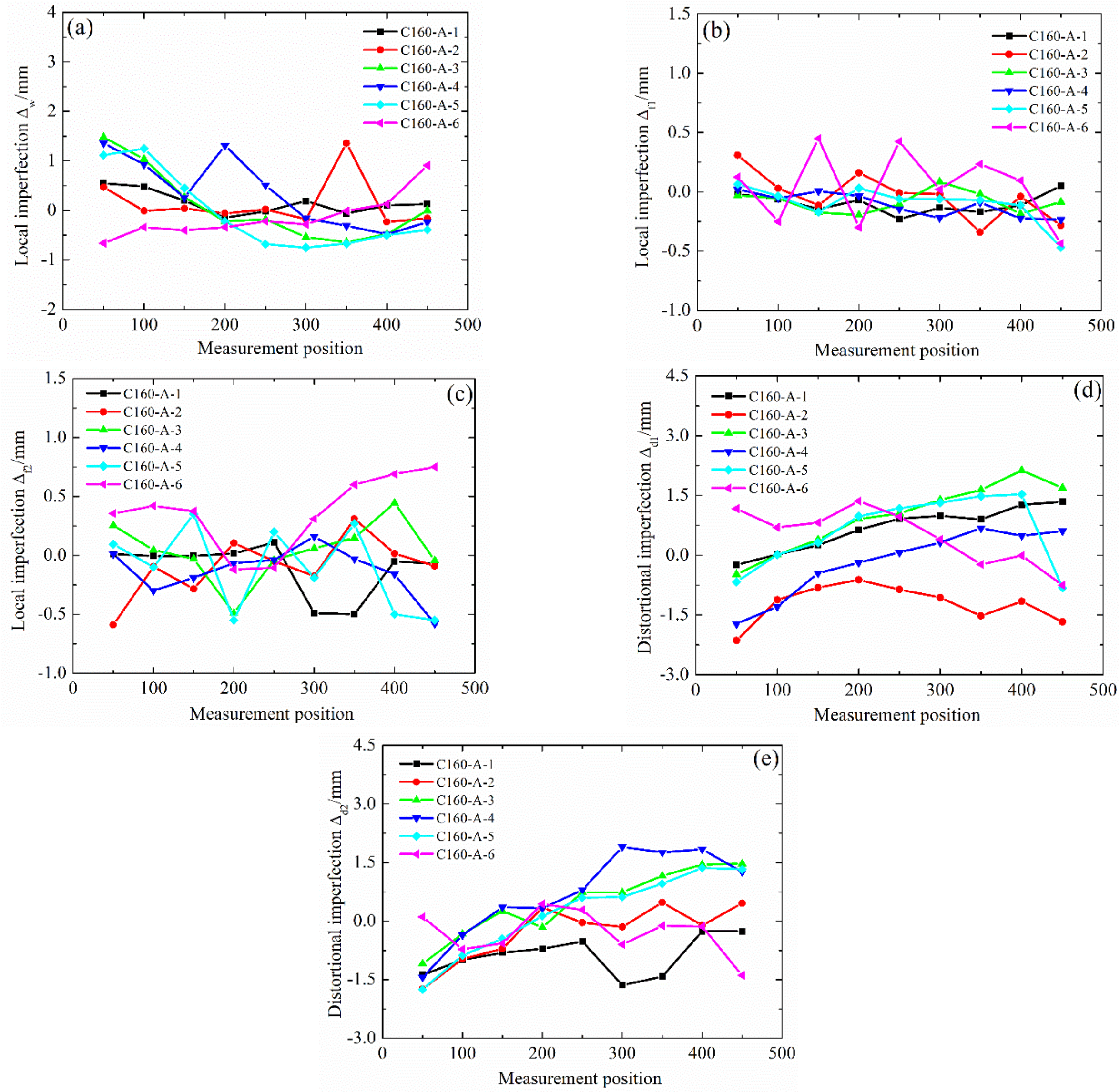


Fig. 7 Initial geometric imperfections along the column length

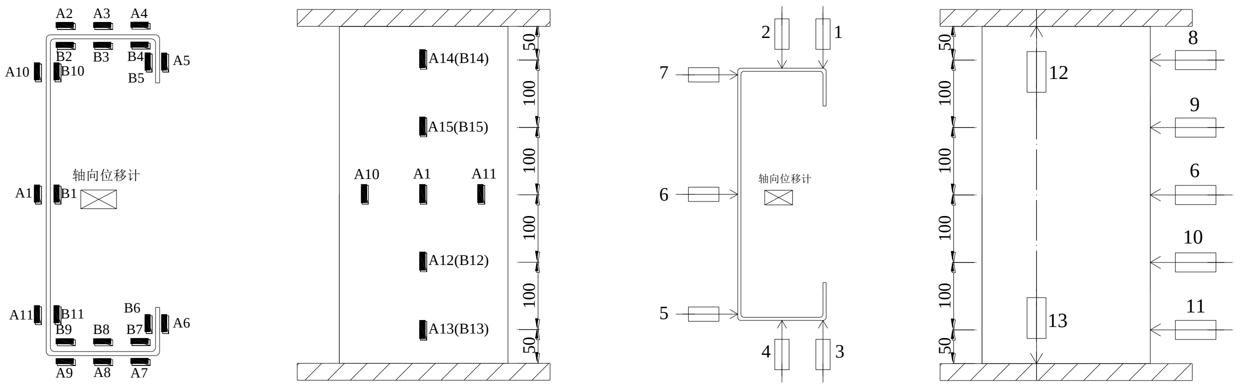


(a) Strain gauge arrangement (b) Displacement transducer arrangement

Fig. 8 Layout of strain gauge and displacement transducer


(a) Test arrangement (b) Bottom knife edge (c) Top knife edge

Fig. 9 Experimental set-up

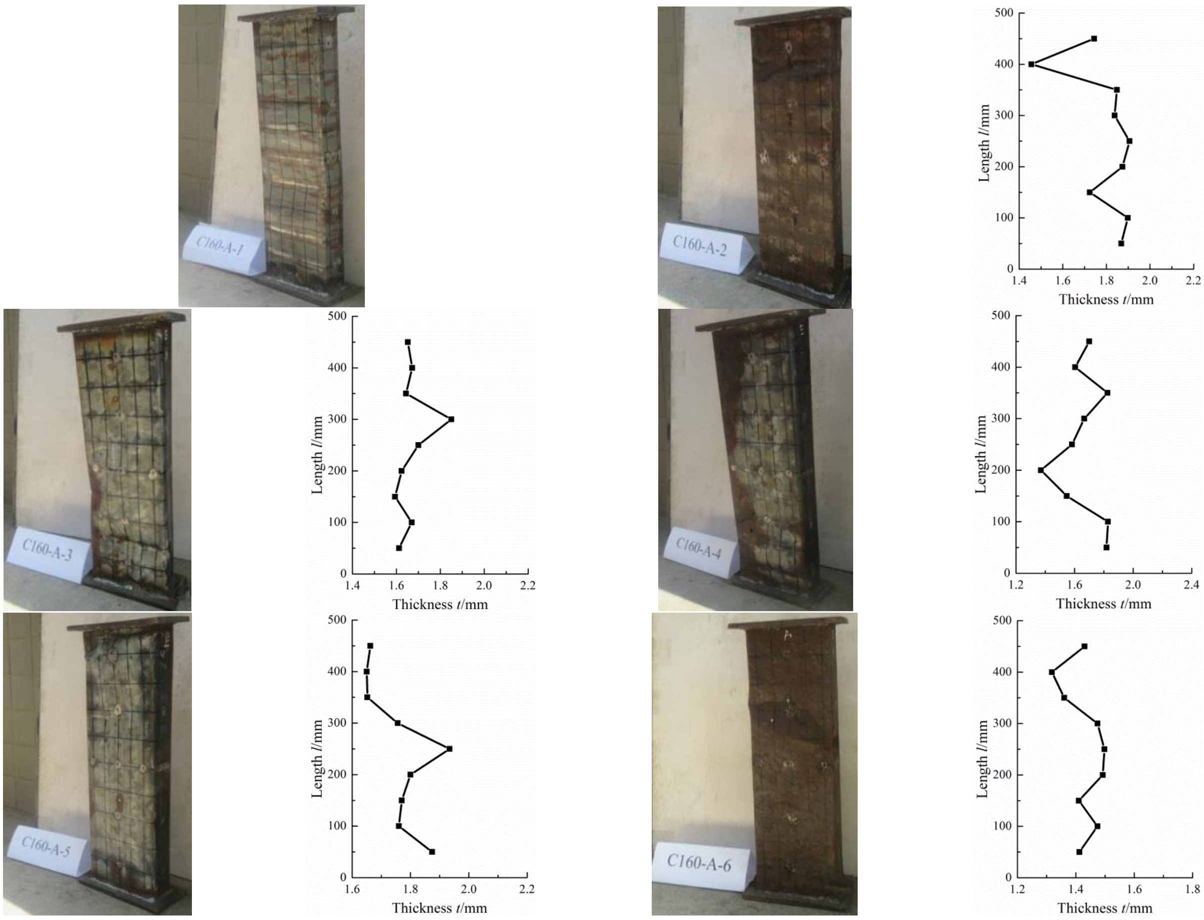


Fig. 10 Failure mode and thickness distribution along the column length

and the applied load was recorded by the force sensor of the machine.

## 4. Experimental results and analysis

### 4.1 Failure mode

The typical failure mode and thickness (the average value of five thicknesses in the same section of web) distribution along the column length is illustrated in Fig. 10. Local buckling was observed in both the corroded and non-corroded columns, and buckling deformation usually occurred in the web, which indicates that corrosion does not change the failure mode in this study. This is because the local buckling wave occurred in the web, which is the weakest part of the non-corroded columns. According to the analysis in Section 3.1, the corrosion of the web is more severe than that of the flange and lip. Therefore, the web of the corroded columns is still weakest part. For the non-corroded columns, no evident deformation was observed when the load was small, and local deformation of the web was not noticeable until the load achieved about 90% of the ultimate load. For the corroded columns, local deformation

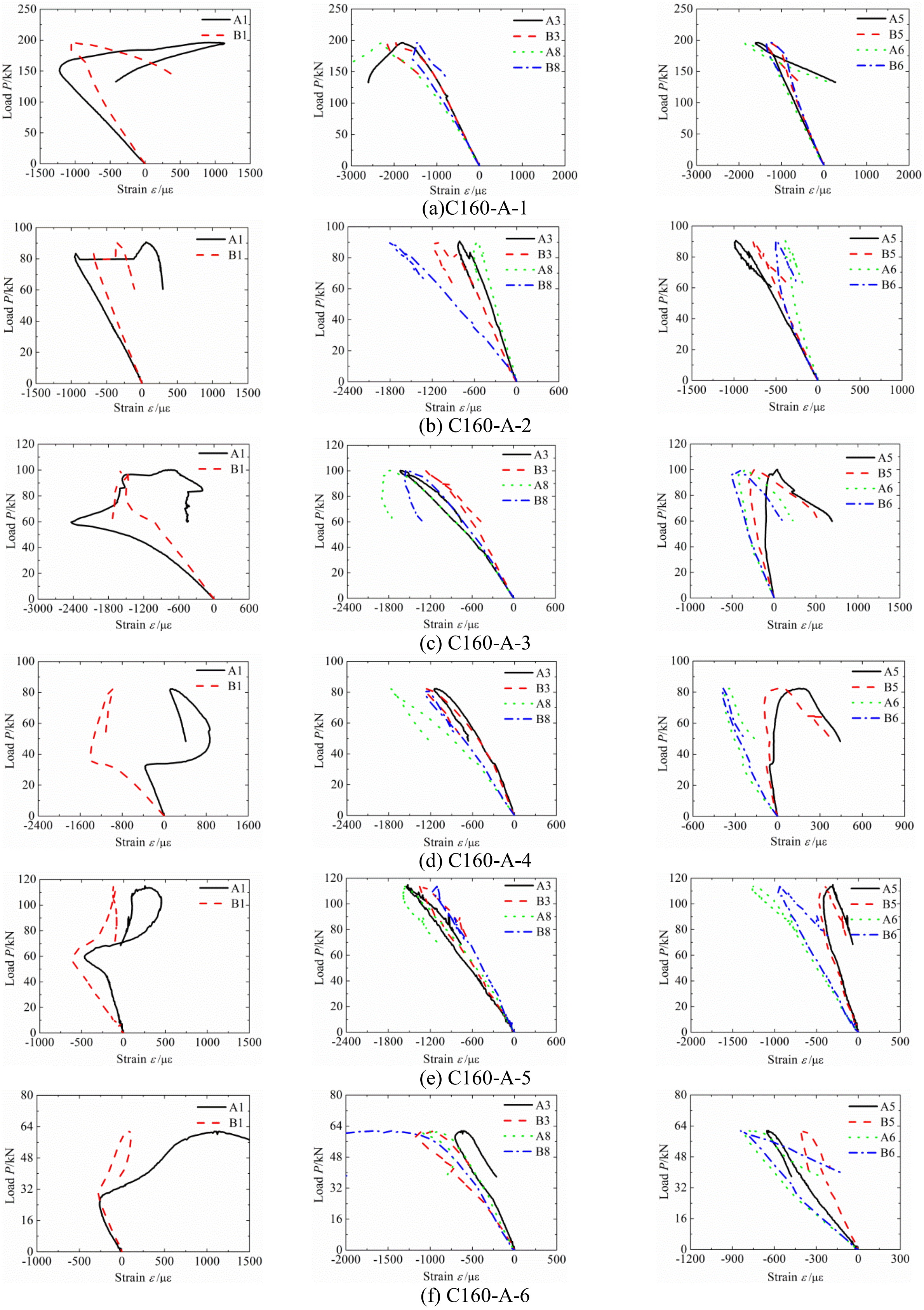

(a)C160-A-1

(b) C160-A-2

(c) C160-A-3

(d) C160-A-4

(e) C160-A-5

(f) C160-A-6

Fig. 11 Load-strain curves of columns

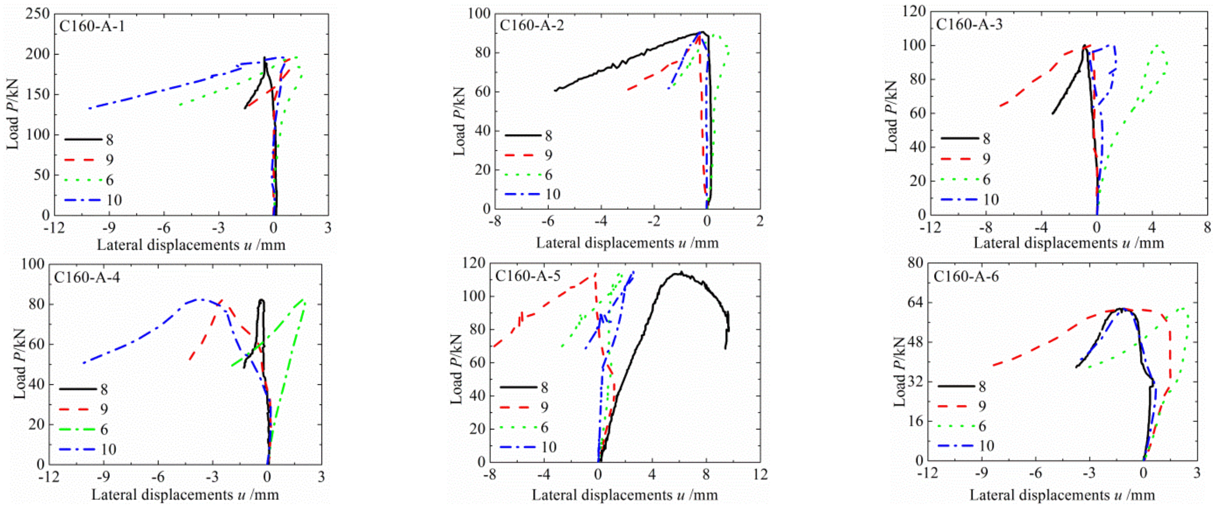


Fig.12 Load-lateral displacement curves of the columns

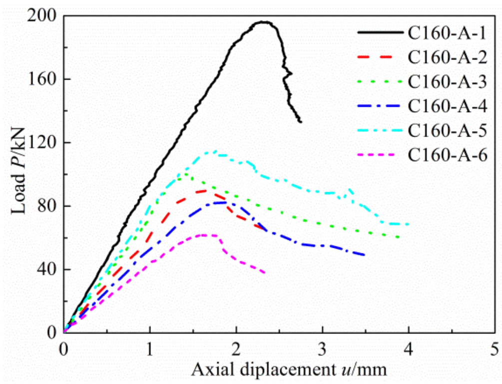


Fig. 13 Load-axial displacement curves of the columns

of the web was observed when the load was only 40% of the ultimate load. This may be because the thickness of the web decreases greatly due to corrosion, which results in a decrease in the critical buckling load and a significant increase in the post-buckling strength. It was also found that the failure positions of the different columns were different. Based on the analysis of the thickness distribution of the columns, the failure positions generally occurred near the section with the minimum web thickness.

### *4.2 Load-strain curves*

The relationship between the axial compression load and the strain of the web (A1,B1), flanges (A3, B3, A8, B8) and lips(A5, B5, A6, B6) of the columns at mid-height are presented in Fig. 11. As shown in Fig.11, the relationship between the axial compression load and the strain was approximately linear at the beginning of the load. With the increase of load, it started to become nonlinear and irregular. The internal and external strains at the same location in the columns were not completely consistent during the initial stage of loading, especially in the web, which may be caused by larger initial geometric imperfections and uneven corrosion. For both the corroded and non-corroded columns, the strain reversal phenomenon was evident in the load-strain curves of the webs, while there was no such phenomenon in the curves of the flanges and lips. This shows that local buckling mainly occurred in the web. In addition, the local buckling of the corroded columns occurred earlier than that of the non-corroded columns.

### *4.3 Load-displacement curves*

The failure position of all the columns is mainly in the web, and the No.11 displacement transducer did not record data because it was broken. Therefore, the axial compression load versus lateral displacement (No.6, 8, 9, 10) is represented in Fig. 12. For all the columns, the lateral displacement was almost non-existent at the beginning of loading. The lateral displacement of the corroded columns was earlier than that of the non-corroded columns. It can also be seen that the lateral displacement of the different positions was quite different because of the initial geometric imperfections and non-uniform corrosion. In addition the lateral displacement corresponding to the ultimate load for

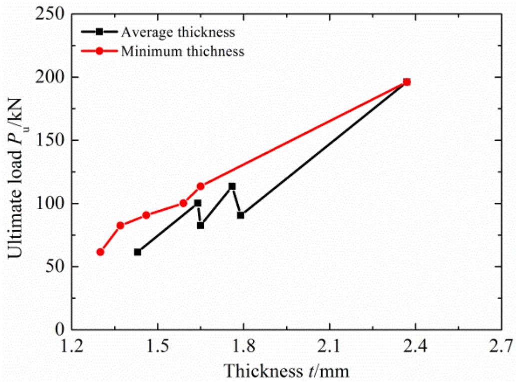


Fig. 14 Ultimate load versus thickness

Table 4 Summary of results for axial compression test

| Specimen | $t_{min}$ | $t_{ave}$ | $\delta$ | $\Delta_u$ /mm | $P_{cr}$/kN | $P_u$/kN | $P_{cr}/P_u$ | $P_u/P_{u0}$ |
|---|---|---|---|---|---|---|---|---|
| C160-A-1 | 2.37 | 2.37 | 0 | 2.36 | 144.81 | 196.10 | 0.73 | 1 |
| C160-A-2 | 1.46 | 1.79 | 0.38 | 1.58 | 80.30 | 90.65 | 0.88 | 0.46 |
| C160-A-3 | 1.59 | 1.64 | 0.32 | 1.42 | 51.72 | 100.20 | 0.51 | 0.51 |
| C160-A-4 | 1.37 | 1.65 | 0.42 | 1.82 | 32.11 | 82.50 | 0.38 | 0.42 |
| C160-A-5 | 1.65 | 1.76 | 0.30 | 1.77 | 57.95 | 113.60 | 0.51 | 0.57 |
| C160-A-6 | 1.30 | 1.43 | 0.45 | 1.59 | 26.52 | 61.50 | 0.43 | 0.31 |

the corroded columns was greater than that for the non-corroded columns. This is due to the thickness loss caused by corrosion

Fig. 13 reports the relationship between the axial compression load and the axial displacement for the columns with different corrosion damage. The shape of the load-axial displacement curves of all the columns was similar, and could be divided into two sections: the ascending section and descending section. The stiffness of ascending section and descending section for the non-corroded columns was obviously larger than that of the corroded columns.

Table 4 summarizes the results for the axial compression test, including the minimum thickness of the web ($t_{min}$), average thickness of the web ($t_{ave}$), axial displacement corresponding to the ultimate load ($\Delta_u$), critical buckling load ($P_{cr}$) and ultimate load ($P_{EXP}$). It is especially important to note that the damage assessment of the corroded CFS components in this paper and that of corroded hot-rolled steel components are different. For corroded hot-rolled steel components, the damage indicator generally comes from the tensile test specimens taken from the corroded components (Xu *et al.* 2019b). However, by analysing the tensile specimens of corroded CFS, it can be found that the damage indicators of the different tensile specimens of the same component vary greatly. The reason for this is that there are great differences in thickness loss at different locations due to the randomness of the environment and materials, and the difference is more obvious for cold-formed thin-walled structures. Therefore, for cold-formed thin-walled steel, it is not suitable to use the performance of a part of the component to represent that of the whole component. To find an appropriate damage indicator, the thickness of the component at different locations was measured. Many studies have shown that average thickness is an important parameter (Beaulieu *et al.* 2010). However the results of this study show that the average thickness was not directly related to the ultimate load (Fig. 14). From Fig. 14, it can be seen that with as the minimum thickness of the web increased, the ultimate load decreased. The above analysis shows that the minimum thickness of the web is an important parameter for determining the mechanical properties of the columns in this paper. Therefore, the thickness loss ratio ($\delta$) defined as the ratio of the minimum thickness of the web ($t_{min}$) to the original thickness ($t_0$) was used as a damage indicator for the corroded columns (see Table 4). It should be noted that the decrease of bearing capacity of corroded specimens is not only due to the decrease of thickness caused by corrosion, but also due to the increase of initial geometric imperfections.

The axial displacement corresponding to the ultimate load for the non-corroded columns was greater than that for the corroded columns, while the change law was not obvious with the increase in the thickness loss ratio. The critical buckling loads of the corroded columns with the thickness loss ratios of 0.38, 0.32, 0.42, 0.30 and 0.45 were about 44.5%, 64.3%, 77.8%, 60.0% and 81.7% lower than those of the non-corroded columns. This indicates that the corrosion has a great influence on the critical buckling load. It also can be seen that the decrease rate of the critical buckling load was greater than that of the ultimate load for the columns with the same thickness loss ratio.

Table 5 Equivalent thickness and comparison of ultimate strength between the test results and the FEA results

| Specimen | $t_{min}$/mm | $t_{max}$/mm | $\alpha$ | $t_{equ}$/mm | $P_{EXP}$/kN | $P_{FEA}$/kN | $P_{EXP}/P_{FEA}$ |
|---|---|---|---|---|---|---|---|
| C160-A-1 | 2.37 | 2.37 | 0 | 2.36 | 196.10 | 195.79 | 1.00 |
| C160-A-2 | 1.46 | 1.90 | 0.76 | 1.68 | 90.65 | 88.05 | 1.02 |
| C160-A-3 | 1.59 | 1.87 | 0.85 | 1.74 | 100.20 | 102.10 | 0.98 |
| C160-A-4 | 1.37 | 1.82 | 0.75 | 1.59 | 82.50 | 78.71 | 1.04 |
| C160-A-5 | 1.65 | 2.05 | 0.80 | 1.86 | 113.60 | 110.22 | 1.03 |
| C160-A-6 | 1.30 | 1.49 | 0.86 | 1.41 | 61.50 | 62.30 | 0.98 |

## 5. Finite element analysis

### 5.1 Finite element model

In this paper, the finite element software ABAQUS was applied to analyse mechanical properties of the corroded CFS columns under an axial compression load. The measured cross-section dimensions and lengths of the test columns (Table 2) were used to establish the finite element models. It is especially important to note that the thickness distribution of the columns is random and the thickness of only part of the position was measured. It is difficult to build a finite element model with a stochastic thickness. Therefore, it is very important to propose a suitable method for finite element analysis of corroded cold-formed columns with uneven corrosion. The appropriate method is to use an equivalent uniform thickness to replace the complex stochastic thickness (Paik *et al.* 2003, Ok *et al.* 2007, Dunbar *et al.* 2004). From the above analysis, it can be found that the minimum thickness of the web was the governing parameter to determine the failure position and the bearing capacity. However, the results of the finite element analysis considering only the minimum thickness were smaller than the test results. The non-uniformity coefficient ( $\alpha$ ) defined as the ratio of the minimum thickness ($t_{min}$) to the maximum thickness ($t_{max}$) was proposed to modify the thickness. Therefore, an equivalent thickness method that considers the minimum thickness and non-uniform thickness loss was proposed. The minimum thickness, maximum thickness and non-uniformity coefficient are reported in Table 5. Based on many finite element analyses and tests results, the equivalent thickness of corroded cold-formed columns can be calculated using the following equation

$$t_{equ} = (1.67 - 0.67 * \alpha) * t_{min} \quad (4)$$

where $t_{equ}$ is the equivalent thickness, $\alpha$ is the non-uniformity coefficient, $t_{min}$ is the minimum thickness

#### 5.1.1 Element type and size

The S4R element, which is suitable for the analysis of linear, large rotation, and/or large strain nonlinear applications, was selected for the buckling analysis of corroded cold-formed columns. The S4R shell element has six degrees of freedom per node, including three rotational degrees of freedom and three translational degrees of freedom. The element size of the finite element model has a significant influence on the results. A mesh sensitivity analysis was carried out for columns with various mesh sizes from 14 mm x 14 mm to 5 mm x 5 mm to study the effect of the different mesh sizes on the results of the finite element analysis. It was shown that the element size of 8 mm x 8 mm was suitable for the analysis of the column with acceptable processing time and precision (Fig. 15).

#### 5.1.2 Boundary conditions and loading

The boundary conditions should simulate the real experimental pinned-end supports. The boundary conditions were applied to the columns through the reference point located at the centre of the cross-section. The top and bottom reference points were connected to the nodes of the top and bottom ends of the columns with all the degrees of freedom rigidly attached to each other. The appropriate finite element boundary conditions are presented in Fig. 15. Three translational degrees of freedom for the bottom reference point were restrained. At the top end, the translational degrees of freedom for the top reference point were restrained in the x and y directions, while the axial translation in the z direction was not restrained. It is worth noting that the rotational degree of freedom in the minor axis must be released. The axial load was applied on the top reference point with the displacement control.

#### 5.1.3 Geometric imperfections and material properties

The initial geometric imperfections of the thin-walled structures have a great influence on the bearing capacity and failure modes. To analyse the failure modes of the experimental columns, the appropriate eigenmode must be applied to the finite element model and usually the lowest eigenmode is appropriate. The initial geometric imperfections used in the FE modelling of corroded cold-formed columns are reported in Table 3. The following parameters for the material properties need to be determined: the elastic modulus, the stress-strain relationship and the Poisson's ratio. The stress-strain curve of the materials was assumed to be a perfect bilinear model, and the slope of the plastic hardening section was 2% of the elastic modulus. The material properties of the tensile coupon specimens taken from the corroded CFS columns are presented in Table 1.

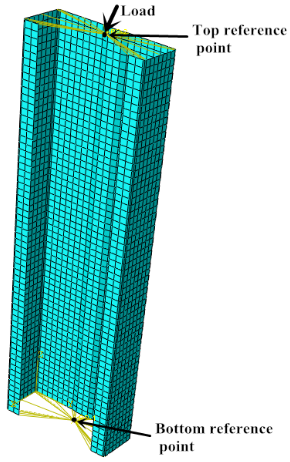


Fig. 15 Finite element model

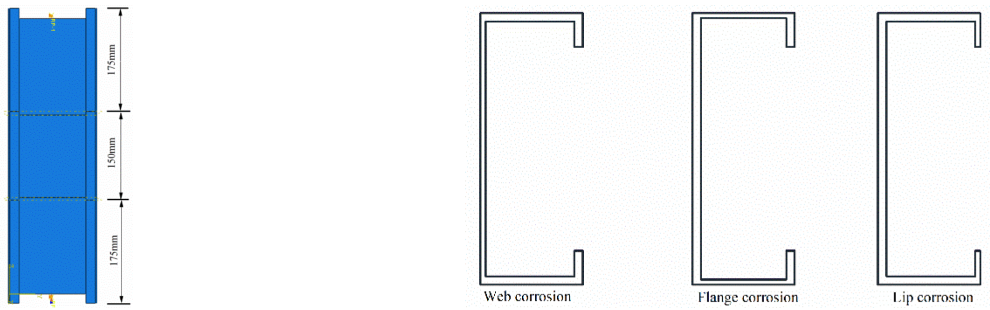


Fig. 16 Localized corrosion location

Table 6 Comparison of ultimate load and failure mode of corroded CFS columns with different corrosion damages

| Specimen | Failure mode | $P_u$/kN | $P_u/P_{u0}$ | Specimen | Failure mode | $P_u$/kN | $P_u/P_{u0}$ |
|---|---|---|---|---|---|---|---|
| C160-W-C0 | L | 309.87 | 1 | C160-F-C1.5 | D | 236.17 | 0.76 |
| C160-W-C0.5 | L | 265.90 | 0.85 | C160-F-C2 | D | 206.70 | 0.66 |
| C160-W-C1 | L | 208.99 | 0.67 | C160-L-C0.5 | L | 309.63 | 1 |
| C160-W-C1.5 | L | 171.77 | 0.55 | C160-L-C1 | L | 307.63 | 0.99 |
| C160-W-C2 | L | 146.43 | 0.47 | C160-L-C1.5 | D | 303.35 | 0.97 |
| C160-F-C0.5 | L | 306.24 | 0.98 | C160-L-C2 | D | 292.05 | 0.94 |
| C160-F-C1 | D | 281.03 | 0.90 | | | | |

*C160-W/F/L-C: C160 is web depth; W, F and L are web, flange and lip, respectively; C is corrosion damage, for example, C160-W-C0.5 is a specimen with 0.5mm reduction of the web thickness

#### *5.1.4 Analysis procedure*

The analysis procedure was divided into two steps: elastic buckling anasysis and non-linear analysis. Elastic buckling analysis was first performed to obtain the appropriate eigenmode for applying the geometric imperfections. Then, non-linear buckling analysis was used to obtain the mechanical properties of the corroded columns by the arc length method.

### *5.2 Validation of the finite element models*

The comparison of the ultimate strength between the test results and the FEA results are reported in Table 5. The mean value of the $P_{EXP}/P_{FEA}$ ratio was 1.01, which shows that there is reasonably good agreement between the test results and the FEA results for corroded CFS columns with different corrosion damage.

### *5.3 Parametric study*

It is now generally believed that two main types of corrosion for a steel member, namely general and localized corrosion. The localized corrosion that causes the thickness of the web, flange or lip to decrease within a zone is very difficult to avoid in actual corrosive environment. Therefore, the influence of localized corrosion on the

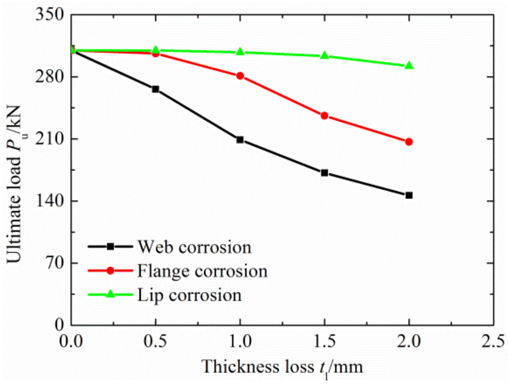


Fig. 17 Ultimate load versus thickness loss for the columns with localized corrosion

Table 7 Comparison of axial capacity between experimental results and results predicted using the existing design specifications

| Specimen | $P_{EXP}$/kN | AISI-DSM | | MOHURD-DSM | |
|---|---|---|---|---|---|
| | | $P_A$/kN | $P_{EXP}/P_A$ | $P_M$/kN | $P_{EXP}/P_M$ |
| C160-A-1 | 196.10 | 183.73 | 1.06 | 212.73 | 0.92 |
| C160-A-2 | 90.65 | 76.72 | 1.18 | 90.83 | 0.99 |
| C160-A-3 | 100.20 | 85.52 | 1.17 | 101.02 | 0.99 |
| C160-A-4 | 82.50 | 67.31 | 1.22 | 79.95 | 1.03 |
| C160-A-5 | 113.60 | 97.55 | 1.16 | 114.81 | 0.98 |
| C160-A-6 | 61.50 | 53.12 | 1.15 | 63.84 | 0.96 |

mechanical properties of CFS columns was analysed by the finite element method. The non-corroded column was the C160×60×20 channel section with a nominal plate thickness of 2.9 mm. This paper mainly studies the localized corrosion in the 150 mm range near the mid-height of the columns (see Fig. 16). The thicknesses of the web, flange and lip were reduced by 0.5 mm, 1 mm, 1.5 mm and 2 mm, respectively.

Comparisons of the ultimate load and failure mode of the corroded CFS columns with different corrosion damage are summarized in Table 7, and the relationship between the ultimate load and the thickness loss for the columns with localized corrosion is depicted in Fig. 17. The following observations can be made:

Local buckling was observed in all the columns with web corrosion, which indicates the web corrosion did not change the failure mode. This is because the web is still a weakest part of the corroded columns. The ultimate load for the columns with a web thickness that decreased by 0.5 mm, 1 mm, 1.5 mm and 2 mm, compared to a non-corroded web was reduced by 15%, 33%, 45% and 53%, respectively. This indicates that web corrosion has a great influence on the bearing capacity of CFS columns.

For the columns with flange corrosion, when the thickness loss reached 1 mm, the failure mode changed from local buckling to distortional buckling. This is because when the flange is not corroded or corroded relatively low, the web, which is the weak section tends to produce local buckling. When the flange becomes weak due to corrosion, the flange tends to experience distortional buckling. The ultimate load for the columns with a flange thickness that decreased by 0.5 mm, 1 mm, 1.5 mm and 2 mm, compared to a non-corroded flanges reduced by 2%, 10%, 24% and 34%, respectively.

As for the columns with lip corrosion, the failure mode of the column changed from local buckling to distortional buckling until the corrosion loss reached 1.5 mm. This is because when the lip becomes weak due to corrosion, the lip tends to experience distortional buckling. The maximum reduction of the ultimate load for the columns with lip corrosion is only 6%, which shows that lip corrosion has a little effect on the bearing capacity of CFS columns even if it changes the failure mode.

## 6. Design rules for corroded CFS columns

The bearing capacity of the CFS columns was predicted in terms of the existing design specifications, including the North American Specification for the Design of Cold-Formed Steel Structural Members (AISI, 2016) and the Chinese Technical Specification for Cold-Formed Steel Structures (MOHURD). The calculation methods for the bearing capacity of the CFS members mainly include the effective width method (EWM) and the direct strength method (DSM). The DSM was applied to predict the axial capacity of corroded CFS columns in this paper.

The elastic modulus and yield strength of the specimens was obtained from the monotonic tensile test (shown in Table 1), and the equivalent thickness was adopted for the thickness of the corroded specimens. Table 7 presents the comparison of the axial capacity between the experimental results and calculation results for the existing design specifications. $P_A$ and $P_M$ represent the bearing capacity predicted using the AISI and MOHURD, respectively. Table 7 also shows the ratio of the axial capacity obtained by the test to that predicted in terms of the existing design specifications. The mean value of the $P_{EXP}/P_M$ ratio was 0.98, which indicates that the prediction is slightly unconservative. However the mean value of the $P_{EXP}/P_A$ ratio was 1.16, which indicates that the prediction is conservative. Comparing the predicted results of the two methods, it can be found that the prediction results using the MOHURD were more accurate than those using the AISI.

## 7. Conclusions

Experimental and numerical investigations on corroded CFS columns with different corrosion degrees are presented in this paper. Eleven tensile coupon specimens, five test columns and thirteen finite element models were reported. The residual thickness and geometric imperfections of all the columns were measured. The mechanical properties of the tensile coupon specimens and the test results of the columns were discussed. The influence of local corrosion on the ultimate load and failure mode of CFS columns was analysed. Finally, the experimentally measured axial capacity was compared with prediction results for the existing design specifications. The following conclusions can be drawn based on the test and numerical results can be drawn:

- With the increase in the average thickness loss ratio, the ultimate strength, elastic modulus and yield strength decreased. The yield strength has a good linear relationship with the average thickness loss ratio.
- Local deformation was not noticeable until the load achieved approximately 90% of the ultimate loads of the non-corroded columns, while local deformation was observed when the load was only 40% of the ultimate load for the corroded columns. The failure position generally occurred near the section of the minimum web thickness. The ultimate load and critical buckling load were reduced by as much as 57% and 81.7%, respectively, compared to that of the non-corroded columns.
- An appropriate finite element model that uses an equivalent uniform thickness to replace the complex stochastic thickness was proposed. The finite element model was validated against the test results and the results show that there is reasonably good agreement between the test results and the FEA results for the corroded CFS columns with different corrosion damage. Web corrosion does not change the failure mode, but flange and lip corrosion may change the failure mode. The ultimate load was reduced by 53% for the columns with a web thickness that decreased by 2 mm compares to those with a non-corroded web, which indicates that the bearing capacity decreases most obviously for the columns with web corrosion. This shows that the corrosion web should be avoided as much as possible in practical engineering.
- The results predicted using the MOHURD were slightly unconservative, while the results predicted using AISI were conservative. Comparing the results of the two methods, it can be found that the results predicted using the MOHURD were more accurate than those predicted using the AISI. It is worth noting that the method of predicting bearing capacity proposed in this paper is only suitable for the channel section of C160x60x20, whether it is suitable for other cross-section forms needs more research.

## Acknowledgements

This work was supported by 13th Five-Year national focus on R & D project of China with Grant No. 2016YFC0701305 and the National Nature Foundation of China with Grant No.51678477.

## References

AISI S100-16 (2016), *North American Specifcation for the Design of Cold-Formed Steel Structural Members*, American Iron and Steel Institute, USA.

Ananthi, G., Roy, K., Chen, B. and Lim, J.B.P. (2019), "Testing, simulation and design of back-to-back built-up cold-formed steel unequal angle sections under axial compression", *Steel. Compos. Struct.*, **33**(4), 595-614. https://doi.org/10.12989/scs.2019.33.4.595.

Beaulieu, L.V., Legeron, F. and Langlois S. (2010), "Compression strength of corroded steel angle members", *J. Struct. Steel Res.*, **66**(11), 1366-1373. https://doi.org/10.1016/j.jcsr.2010.05.006.

Chen, B., Roy, K., Uzzaman, A., Raftery, G.M., Nash, D., Clifton, G.C. and Lim, J.B. (2019), "Effects of edge-stiffened web openings on the behaviour of cold-formed steel channel sections under compression", *Thin-Wall. Struct.*, **144**, 106307. https://10.1016/j.tws.2019.106307.

Cinitha, A., Umesha, P.K. and Iyer, N.R. (2014), "An overview of corrosion and experimental studies on corroded mild steel compression members", *KSCE J. Civ. Eng. Archit.*, **18**(6), 1735-1744. https://doi.org/10.1007/s12205-014-0362-0.

Cinitha, A., Umesha, P.K., Palani, G.S. and Sampath, V. (2018), "Compression behaviour of ssteel tubular members under simulated corrosion and elevated temperature", *Int. J. Steel Struct.*, **18**(1), 139-152. https://doi.org/10.1007/s13296-018-0311-8.

Dunbar, T.E., Pegg, N., Taheri, F. and Jiang, L. (2004), "A computational investigation of the effects of localized corrosion on plates and stiffened panels", *Mar. Struct.*, **17**, 385-402. https://doi.org/10.1016/j.marstruc.2004.08.012.

Garbatov, Y., Soares, C.G., Parunov, J. and Kodvanj, J. (2014), "Tensile strength assessment of corroded small scale specimens", *Corros. Sci.*, **85**, 296-303. https://doi.org/10.1016/j.corsci.2014.04.031.

Karagah, H., Shi, C., Dawood, M., and Belarbi A. (2015), "Experimental investigation of short steel columns with localized corrosion", *Thin-Wall. Struct.*, **87**, 191-199. https://doi.org/10.1016/j.tws.2014.11.009.

Khurram, N., Sasaki, E., Katsuchi, H. and Yamada, H. (2014), "Experimental and numerical evaluation of bearing capacity of steel plate girder affected by end panel corrosion", *Int. J. Steel*

*Struct.*, **14**(3), 659-676. http://dx.doi.org/10.1007/s13296-015-3018-0.

Kim, I.T., Lee, M.J., Ah, J.H. and Kainuma, S. (2013), "Experimental evaluation of shear buckling behaviors and strength of locally corroded web", *J. Struct. Steel Res.*, **83**, 75-89. https://doi.org/10.1016/j.jcsr.2012.12.015.

Li, J., Li, M. and Sun, Z. (1999), "Development of an artificial climatic complex accelerated corrosion tester and investigation of complex accelerated corrosion test methods", *Corrosion*, **55** (5), 498-502. https://doi.org/10.5006/1.3284012.

Melchers, R.E. and Wells, T. (2006), "Models for the anaerobic phases of marine immersion corrosion", *Corros. Sci.*, **48**, 1791-1811. https://doi.org/10.1016/j.corsci.2005.05.039.

Nakai, T., Matsushita, H., Yamamoto, N. and Arai, H. (2004), "Effect of pitting corrosion on local strength of hold frames of bulk carriers (1st report)", *Mar. Struct.*, **17**, 403-432. https://doi.org/10.1016/j.marstruc.2004.10.001.

Nakhaie, D. and Moayed, M.H. (2014), "Pitting corrosion of cold rolled solution treated 17-4 PH stainless steel", *Corros. Sci.*, **80**, 290-298. https://doi.org/10.1016/S0010-938X(78)80086-9.

Nie, B., Xu, S., Yu, J. and Zhang, H.J. (2019), "Experimental investigation of mechanical properties of corroded cold-formed steels", *J. Struct. Steel Res.*, **162**, 105706. https://doi.org/10.1016/j.jcsr.2019.105706.

Ok, D., Pu, Y. and Incecik, A. (2007), "Computation of ultimate strength of locally corroded unstiffened plates under uniaxial compression", *Mar. Struct.*, **20**, 100-114. https://doi.org/10.1016/j.marstruc.2007.02.003.

Paik, J.K., Lee, J.M. and Ko, M.J. (2003), "Ultimate strength of plate elements with pit corrosion wastage", *J. Eng. Marit. Environ.*, **217**, 185-200. https://doi.org/10.1177/147509020321700402.

Qin, G., Xu, S., Yao, D. and Zhang, Z. (2016), "Study on the degradation of mechanical properties of corroded steel plates based on surface topography", *J. Struct. Steel Res.*, **125**, 205-217. https://doi.org/10.1016/j.jcsr.2016.06.018.

Qiu, B. and Xu, S. (2014), "Degradation law of mechanical properties of corroded steel plates", *Mech. Eng. Mater.,* **38**, 60-63. https://doi.org/1000-3738(2014)10-0060-04

Rahgozar, R. (2009), "Remaining capacity assessment of corrosion damaged beams using minimum curves", *J. Struct. Steel Res.*, **65**(2), 299-307. https://doi.org/10.1016/j.jcsr.2008.02.004.

Roy, K., Lau, H.H. and Lim, J.B.P. (2019a), "Finite element modelling of back-to-back built-up cold-formed stainless-steel lipped channels under axial compression", *Steel. Compos. Struct.*, **33**(1), 869-898. https://doi.org/10.12989/scs.2019.33.1.869.

Roy, K., Ting, T.C., Lau, H.H. and Lim, J.B. (2019b), "Experimental and numerical investigations on the axial capacity of cold-formed steel built-up box sections", *J. Struct. Steel Res.*, (160), 411-427.

Roy, K., Ting, T., Lau, H.H. and Lim, J.B. (2018), "Nonlinear behavior of axially loaded back-to-back built-up cold-formed steel un-lipped channel sections", *Steel. Compos. Struct.*, **28**(2), 233-250. https://doi.org/10.12989/scs.2018.28.2.233.

Saad-Eldee, S., Garbatov, Y. and Soares, C.G. (2012), "Effect of corrosion degradation on ultimate strength of steel box girders", *Corros. Eng. Sci. Technol.*, **47**(4), 272-283. https://doi.org/10.1179/1743278212Y.0000000005.

Sharifi, Y. and Rahgozar, R. (2010), "Remaining moment capacity of corroded steel beams", *Int. J. Steel Struct.*, **10**(2), 165-176. http://dx.doi.org/10.1007/BF03215828.

Sheng, J. and Xia, J. (2017), "Effect of simulated pitting corrosion on the tensile properties of steel", *Constr. Build. Mater.*, **131**, 90-100. https://doi.org/10.1016/j.conbuildmat.2016.11.037.

Shi, C., Karagah, H., Dawood, M. and Belarbi, A. (2014), "Numerical investigation of H-shaped short steel piles with localized severe corrosion", *Eng. Struct.*, **73**, 114-124. https://doi.org/10.1016/j.engstruct.2014.04.048.

Štefec, R. and Franz, F. (1978), "A study of the pitting corrosion of cold-worked stainless steel", *Corros. Sci.*, **18**, 161-168.

Wang, H., Yu, Y., Yu, J.X., Duan, H., Zhang, Y., Li, Z.M. and Wang, C.M. (2018), "Effect of 3D random pitting defects on the collapse pressure of pipe—Part I: Experiment", *Thin-Wall. Struct.*, **129**, 512-526. https://doi.org/10.1016/j.tws.2018.04.015.

Wang, Y., Xu, S. and Li A. (2020b), "Flexural performance evaluation of corroded steel beam based on 3D corrosion morphology", *Struct. Infrastruct. Eng.*, (4), 1-16. https://10.1080/15732479.2020.1713169.

Wang, Y., Xu, S., Li, H. and Zhang, H. (2020a), "Surface characteristics and stochastic model of corroded structural steel under general atmospheric environment", *Acta Metall. Sin.*, **56**(2), 148-160. https://10.11900/0412.1961.2019.00156.

Wang, Y., Xu, S., Wang, H. and Li, A. (2017), "Predicting the residual strength and deformability of corroded steel plate based on the corrosion morphology", *Constr. Build. Mater.*, **152**, 777-793. https://doi.org/10.1016/j.conbuildmat.2017.07.035.

Wu, H., Lei, H., Chen, Y.F. and Qiao, J. (2019), "Comparison on corrosion behaviour and mechanical properties of structural steel exposed between urban industrial atmosphere and laboratory simulated environment", *Constr. Build. Mater*, 211, 228-243. https://doi.org/10.1016/j.conbuildmat.2019.03.207.

Xu, S., Zhang, Z. and Qin, G. (2019b), "Study on the seismic performance of corroded H-shaped steel columns", *Eng. Struct.*, **191**, 39-61. https://doi.org/10.1016/j.engstruct.2019.04.037.

Xu, S., Zhang, Z., Li, R. and Wang, H. (2019a), "Effect of cleaned corrosion surface topography on mechanical properties of cold-formed thin-walled steel", *Constr. Build. Mater.*, **222**, 1-14. https://doi.org/10.1016/j.conbuildmat.2019.06.130.

Zhang, Z., Xu, S. and Li, R. (2020a), "Comparative investigation of the effect of corrosion on the mechanical properties of different parts of thin-walled steel", *Thin-Wall. Struct.*, **146**, 106450, https://10.1016/j.tws.2019.106450.

Zhang, Z., Xu, S., Nie, B. and Xing Z. (2020b), "Experimental and numerical investigation of corroded steel columns subjected to in-plane compression and bending", *Thin-Wall. Struct.*, **151**, 106735, https://10.1016/j.tws.2020.106735.

Zhou, X. and Chen, M. (2018), "Experimental investigation and finite element analysis of web-stiffened cold-formed steel columns with batten sheets", *Thin-Wall. Struct.*, **125**, 38-50. https://doi.org/10.1016/j.tws.2018.01.006.

*CC*